Chapter 5

Numerical solution of two-dimensional non-linear Riesz space-fractional reaction-advection-diffusion equation using fast compact implicit integration factor method

5.1 Introduction

Lately, many researchers are interested to use the fractional calculus in multiple fields like mathematical modeling in physics [145], [146], [75], groundwater contaminant transport [60], [93] and in solving fractional advection-dispersion equation

The contents of this chapter have been accepted in **Journal of Applied Mathematics and Mechanics.**

problems. Reaction-diffusion equations (due to its capabilities to model several processes in various fields) have been widely studied in last few years, in various forms viz., biological pattern formation [147], heterogeneous networks [148], avascular tumor growth [149], forest fire propagation [150], cancer invasion [151]. Over the last few years, the classical reaction-diffusion equations have been expanded to represent the fractional reaction-diffusion equations [152], [153], [5] to model pattern formation in inhomogeneous media. Henry et al.[154] have discussed the diffusion problem with linear reaction using a continuous-time random walk model. Many numerical methods exist in literature survey to solve fractional diffusion equation like [95], [100], [93], [155], [156]. Various models for nonlinear situations were discovered throughout the literature review like [83], [84], [85], [82]. In this chapter, the following two-dimensional non-linear fractional order partial differential equation with Riesz space fractional derivative (FPDE-RSFD) is considered as

$$\frac{\partial u(x,y,t)}{\partial t} = D\left(\frac{\partial^{\beta+1}u(x,y,t)}{\partial|x|^{\beta+1}} + \frac{\partial^{\beta+1}u(x,y,t)}{\partial|y|^{\beta+1}}\right) - V_x\frac{\partial^{\beta}u(x,y,t)}{\partial|x|^{\beta}} - V_y\frac{\partial^{\beta}u(x,y,t)}{\partial|y|^{\beta}} + f(u),\ 0<\beta<1, \tag{5.1}$$

where $u(x,y,t)$ represents a solute concentration, D is the dispersion coefficient, V_x and V_y are the advection coefficients of fluid flow along $x-$ and $y-$ directions, respectively and $f(u)$ is the non-linear reaction term, and $(x,y)\in\Omega$ and $t\in[0,T]$, $\Omega=(a,b)\times(c,d)$ and $\partial\Omega$ is the boundary of Ω. The initial and boundary conditions are considered as

$$u(x,y,0) = u_0(x,y),\ (x,y)\in\Omega, \tag{5.2}$$

$$u(x,y,t) = 0,\ (x,y)\in\partial\Omega,\ 0<t\leq T. \tag{5.3}$$

In the equation (5.1), the parameter β $(0 < \beta < 1)$ is known as the Riesz space fractional derivative. When $\beta = 1$, the concerned system (5.1) reduces to the classical reaction-advection-dispersion equation (RADE). Here two cases are considered, firstly the case when $V_x = V_y = 0$ for which the equation (5.1) reduces to two-dimensional non-linear SFRDE [157]. Secondly when $V_x \neq 0$, $V_y \neq 0$, the equation (5.1) reduces to a two-dimensional non-linear SFRADE [158]. A numerical method is proposed to approximate the Riesz space fractional derivative by using the shifted Grünwald method and then the method given in [159] is used to solve the concerned mathematical model.

The kinetics of chaotic dynamics have been used to develop the Riesz fractional derivative [157]. The space-fractional derivative is usually referred to as the Riesz derivative since it is formulated as an operator inverse to the Riesz potential [160]. Riesz fractional derivative allows us to find fractional order derivative of any continuous function. More can be found about Riesz fractional derivative in the article [161].

5.2 Spatial discretization using WSGD Difference Scheme

In this section, the non-linear equation SFRADE given in equation (5.1) is spatially discretized. It is noticed that SFRDE can be spatially discretized by putting $V_x = V_y = 0$ in equation (5.1). Let the spatial grid sizes be $h_1 = (b-a)/N_1$ and $h_2 = (d-c)/N_2$ in the $x-$ and $y-$ directions, respectively, where N_1 and N_2 are some natural numbers i.e., intervals (a, b) and (c, d) are divided into N_1 and N_2 number of sub-intervals. Then spatial partition will be $x_i = a + ih_1$, $i = 0, 1, ..., N_1$ and $y_j = c + jh_2$, $j = 0, 1, ..., N_2$. Using the definition 2.3 of the previous section

to discretize the left and right Riemann-Liouville space fractional derivatives in $x-$ direction (for $0 < \beta < 1$ exponent part), we get

$$ {}_aD_x^{\beta}u(x_i, y_j) = \frac{1}{h_1^{\beta}} \sum_{k=0}^{i+1} \omega_k^{\beta} u(x_{i-k+1}, y_j) + O(h^p), \tag{5.4} $$

$$ {}_xD_b^{\beta}u(x_i, y_j) = \frac{1}{h_1^{\beta}} \sum_{k=0}^{N_1-i+1} \omega_k^{\beta} u(x_{i+k-1}, y_j) + O(h^p). \tag{5.5} $$

Similarly, discretization of the left and right Riemann-Liouville space fractional order derivatives in $y-$ direction can be derived. From [1], if $\beta = 1$, the Grünwald-Letnikov formulae (5.4) and (5.5) reduces to the back forward difference method.

To discretize the left and right Riemann-Liouville space fractional derivatives in $x-$ direction (for $1 < \beta + 1 < 2$ exponent part), we use

$$ {}_aD_x^{\beta+1}u(x_i, y_j) = \frac{1}{h_1^{\beta+1}} \sum_{k=0}^{i+1} \omega_k^{\beta+1} u(x_{i-k+1}, y_j) + O(h^p), \tag{5.6} $$

$$ {}_xD_b^{\beta+1}u(x_i, y_j) = \frac{1}{h_1^{\beta+1}} \sum_{k=0}^{N_1-i+1} \omega_k^{\beta+1} u(x_{i+k-1}, y_j) + O(h^p). \tag{5.7} $$

Similarly discretization of the left and right Riemann-Liouville space fractional derivatives can be derived in $y-$ direction. From [1], the formula used in equation (5.6) and (5.7) reduces to the central difference method for $\beta + 1 = 2$.

Now let $u \in C^4(R^2)$, then from [1] we can get equations (5.6) and (5.7) for accuracy of second- order i.e., $p = 2$ and coefficients $\omega_k^{\beta+1}$ given in (5.6) and (5.7) are obtained as

$$ \omega_0^{\beta+1} = \frac{\beta+1}{2} d_0^{\beta+1}, \; \omega_k^{\beta+1} = \frac{\beta+1}{2} d_k^{\beta+1} + \frac{(2-\beta+1)}{2} d_{k-1}^{\beta+1}, \tag{5.8} $$

where $d_0^{\beta+1} = 1$ and $d_k^{\beta+1} = (1 - \frac{1+\beta+1}{k}) d_{k-1}^{\beta+1}$.

After substituting these equations for exponent β in equations (5.4), (5.5) and then

substituting it in equation (5.4), we get

$$\frac{\partial^\beta u}{\partial|x|^\beta} = \frac{-1}{2h_1^\beta cos(\beta\pi/2)}(\sum_{k=0}^{i+1}\omega_k^\beta u(x_{i-k+1},y_j) + \sum_{k=0}^{N_1-i+1}\omega_k^\beta u(x_{i+k-1},y_j)) + O(h^p). \quad (5.9)$$

Similarly, one can find in $y-$direction. Now substituting equation (5.8) in equations (5.6), (5.7) and then substituting it in equation (1.16) for exponent $\beta+1$, we get

$$\frac{\partial^{\beta+1} u}{\partial|x|^{\beta+1}} = \frac{-1}{2h_1^{\beta+1}cos((\beta+1)\pi/2)}(\sum_{k=0}^{i+1}\omega_k^{\beta+1}u(x_{i-k+1},y_j) + \sum_{k=0}^{N_1-i+1}\omega_k^{\beta+1}u(x_{i+k-1},y_j)) + O(h^p). \quad (5.10)$$

Now to discretize the system (5.1), suppose the numerical approximation of $u(x_i,y_j)$ is u_{ij}, and then with appropriate substitution for $x-$ and $y-$ direction in the expression given in equations (5.9) and (5.10), and then substituting it in equation (5.1), we get

$$\begin{aligned}\frac{\partial u_{ij}}{\partial t} = &-\frac{D}{2h_1^{\beta+1}cos((\beta+1)\pi/2)}(\sum_{k=0}^{i+1}\omega_k^{\beta+1}u(x_{i-k+1},y_j) + \sum_{k=0}^{N_1-i+1}\omega_k^{\beta+1}u(x_{i+k-1},y_j))\\ &-\frac{D}{2h_2^{\beta+1}cos((\beta+1)\pi/2)}(\sum_{k=0}^{j+1}\omega_k^{\beta+1}u(x_i,y_{j-k+1}) + \sum_{k=0}^{N_2-j+1}\omega_k^{\beta+1}u(x_i,y_{j+k-1}))\\ &+\frac{V_x}{2h_1^\beta cos(\beta\pi/2)}(\sum_{k=0}^{i+1}\omega_k^\beta u(x_{i-k+1},y_j) + \sum_{k=0}^{N_1-i+1}\omega_k^\beta u(x_{i+k-1},y_j))\\ &+\frac{V_y}{2h_2^\beta cos(\beta\pi/2)}(\sum_{k=0}^{j+1}\omega_k^\beta u(x_i,y_{j-k+1}) + \sum_{k=0}^{N_2-j+1}\omega_k^\beta u(x_i,y_{j+k-1})) + f(u_{ij}). \quad (5.11)\end{aligned}$$

Now denoting $U = \begin{pmatrix} u_{11} & u_{12} & \dots & u_{1(N_2-1)} \\ u_{21} & u_{22} & \dots & u_{2(N_2-1)} \\ \vdots & \vdots & \ddots & \vdots \\ u_{(N_1-1)1} & u_{(N_1-1)2} & \dots & u_{(N_1-1)(N_2-1)} \end{pmatrix}$,

$$U_0 = \begin{pmatrix} u_0(x_1,y_1) & u_0(x_1,y_2) & ... & u_0(x_1,y_{N_2-1}) \\ u_0(x_2,y_1) & u_0(x_2,y_2) & ... & u_0(x_2,y_{N_2-1}) \\ \vdots & \vdots & \ddots & \vdots \\ u_0(x_{N_1-1},y_1) & u_0(x_{N_1-1},y_2) & ... & u_0(x_{N_1-1},y_{N_2-1}) \end{pmatrix},$$

$$W_N^{\beta+1} = \begin{pmatrix} 2\omega_1^{\beta+1} & \omega_0^{\beta+1}+\omega_2^{\beta+1} & \omega_3^{\beta+1}... & \omega_{N-1}^{\beta+1} \\ \omega_0^{\beta+1}+\omega_2^{\beta+1} & 2\omega_1^{\beta+1} & \omega_0^{\beta+1}+\omega_2^{\beta+1}... & \omega_{N-2}^{\beta+1} \\ \omega_3^{\beta+1} & \omega_0^{\beta+1}+\omega_2^{\beta+1} & 2\omega_1^{\beta+1}... & \omega_{N-3}^{\beta+1} \\ \vdots & \vdots & \ddots & \vdots \\ \omega_{N-2}^{\beta+1} & \omega_{N-3}^{\beta+1} & \omega_{N-4}^{\beta+1}... & \omega_0^{\beta+1}+\omega_2^{\beta+1} \\ \omega_{N-1}^{\beta+1} & \omega_{N-2}^{\beta+1} & \omega_{N-3}^{\beta+1}... & 2\omega_1^{\beta+1} \end{pmatrix}$$

and

$$W_N^{\beta} = \begin{pmatrix} 2\omega_1^{\beta} & \omega_0^{\beta}+\omega_2^{\beta} & \omega_3^{\beta}... & \omega_{N-1}^{\beta} \\ \omega_0^{\beta}+\omega_2^{\beta} & 2\omega_1^{\beta} & \omega_0^{\beta}+\omega_2^{\beta}... & \omega_{N-2}^{\beta} \\ \omega_3^{\beta} & \omega_0^{\beta}+\omega_2^{\beta} & 2\omega_1^{\beta}... & \omega_{N-3}^{\beta} \\ \vdots & \vdots & \ddots & \vdots \\ \omega_{N-2}^{\beta} & \omega_{N-3}^{\beta} & \omega_{N-4}^{\beta}... & \omega_0^{\beta}+\omega_2^{\beta} \\ \omega_{N-1}^{\beta} & \omega_{N-2}^{\beta} & \omega_{N-3}^{\beta}... & 2\omega_1^{\beta} \end{pmatrix},$$

the equation (5.11) can be converted in the matrix form as

$$\frac{dU}{dt} = A_1U + UD_1 + C_1U + UB_1 + F(U), \tag{5.12}$$

with $U(0) = U_0$, in which

$$A_1 = \frac{-D}{2h_1^{\beta+1}cos((\beta+1)\pi/2)}W_{N_1}^{\beta+1},\ B_1 = \frac{V_y}{2h_2^{\beta}cos(\beta\pi/2)}W_{N_2}^{\beta},$$
$$C_1 = \frac{V_x}{2h_1^{\beta}cos(\beta\pi/2)}W_{N_1}^{\beta},\ D_1 = \frac{-D}{2h_2^{\beta+1}cos((\beta+1)\pi/2)}W_{N_2}^{\beta+1},$$

where $W_{N_1}^{\beta+1}$, $W_{N_2}^{\beta}$, $W_{N_1}^{\beta}$, $W_{N_2}^{\beta+1}$ can easily be calculated by replacing N in $W_N^{\beta+1}$ and W_N^{β} by N_1 and N_2. If we substitute $A = A_1 + C_1$ and $B = B_1 + D_1$, we get

$$\frac{dU}{dt} = AU + UB + F(U), \tag{5.13}$$

with $U(0) = U_0$.

5.3 Derivation of the FcIIF method with non-uniform time meshes.

From the Proposition 2.1 in [159], since $W_N^{\beta+1}$ is negative definite and W_N^{β} is positive definite for $0 < \beta < 1$, the matrices A and B are positive definite matrices. We know that a positive definite matrix can be written as a product form. Therefore, $A = P_A D_A P_A^T$ and $B = P_B D_B P_B^T$, where D_A and D_B are diagonal matrices whose diagonal elements are the eigenvalues of A and B, respectively, P_A and P_B are orthogonal matrices, respectively. Substituting A and B in equation (5.13), we get

$$\frac{dU}{dt} = (P_A D_A P_A^T)U + U(P_B D_B P_B^T) + F(U).$$

Now pre and post multiplying by P_A^T and P_B, respectively, we obtain

$$\frac{d(P_A^T U P_B)}{dt} = D_A(P_A^T U P_B) + (P_A^T U P_B)D_B + P_A^T F(U) P_B.$$

After substituting $V = P_A^T U P_B$ and $H = P_A^T F P_B$, we get

$$\frac{dV}{dt} = D_A V + V D_B + H(P_A V P_B^T).$$

The integration on both sides is performed, to calculate V and in order to do so, first we pre and post multiply both sides by $e^{-D_A t}$ and $e^{-D_B t}$, respectively,

$$e^{-D_A t}\frac{dV}{dt}e^{-D_B t} = e^{-D_A t}(D_A V + V D_B + H(P_A V P_B^T))e^{-D_B t}. \tag{5.14}$$

After simple calculation, as in [159], we get

$$\frac{d(e^{-D_A t}Ve^{-D_B t})}{dt} = e^{-D_A t}H(P_A V P_B^T)e^{-D_B t}.$$

Integrating both sides from t_n to t_{n+1}, where $t_{n+1} = t_n + \Delta t_n$, we obtain

$$\int_{t_n}^{t_{n+1}} d(e^{-D_A t}V(t)e^{-D_B t}) = \int_{t_n}^{t_{n+1}} e^{-D_A \tau}H(P_A V P_B^T)e^{-D_B \tau}d\tau.$$

Changing limits of integration from $t_n \to t_{n+1}$ to $0 \to \Delta t_n$, we obtain

$$\int_{0}^{\Delta t_n} d(e^{-D_A t}V(t_n + t)e^{-D_B t}) = \int_{0}^{\Delta t_n} e^{-D_A \tau}H(P_A V(t_n + \tau)P_B^T)e^{-D_B \tau}d\tau.$$

Thus,

$$e^{-D_A t_n}V_{n+1}e^{-D_B t_n} = V_n + \int_{0}^{\Delta t_n} e^{-D_A \tau}H(P_A V(t_n + \tau)P_B^T)e^{-D_B \tau}d\tau,$$

As calculated in [159], we now get

$$V_{n+1} = E_{AB}^n \odot V_n + \Delta t_n(H(P_A V_{n+1}P_B^T)\alpha_1 + \sum_{i=2-r}^{0} E_{AB}^{n+i}H(P_A V_{n+i}P_B^T)\alpha_i). \tag{5.15}$$

For second-order ($r = 2$), we get

$$V_{n+1} = E_{AB}^n \odot V_n + \Delta t_n \alpha_0 H(P_A V_n P_B^T) + \Delta t_n \alpha_1 H(P_A V_{n+1} P_B^T), \tag{5.16}$$

where $\alpha_1 = \alpha_0 = 1/2$.

The time step sizes in equation (5.16) are non-uniform and the accuracy of the numerical solutions for the non-uniform time meshes are more as compared to those for uniform meshes [162]. Even, numerical methods using non-uniform meshes can achieve ideal accuracy, which can strongly reduce the computational cost. After finding V_n, we can calculate U_n since $V_n = P_A^T U_n P_B$. For the proposed FcIIF method for the system (5.1), it does not involve complex matrices those can increase computational time and cost, because one can deal with diagonal matrices, for every time step. As a result, less computational time and less CPU cost will be spent to get more accurate results.

5.4 Numerical Simulation

In this section, the proposed numerical scheme is used on two existing problems to find the approximate numerical solutions. The obtained results are compared with the analytic results in tabular and graphical forms through finding the L^∞-errors to illustrate the effectiveness of the proposed scheme. The L^∞-error in $0 \leq x \leq 1$ for fixed values of y and t is defined as

$$Er_\infty = ||u_{exact}(x, 0.5, 0.5) - u_{k,k,k}(x, 0.5, 0.5)||_\infty$$

$$= \sup_{0 \leq x \leq 1} |u_{exact}(x, 0.5, 0.5) - u_{k,k,k}(x, 0.5, 0.5)|.$$

The rate of convergence (μ_k) is calculated using the formula

$$\mu_k = \frac{||u(x, 0.5, 0.5) - u_{2^{k+3},2^{k+3},2^{k+3}}(x, 0.5, 0.5)||_\infty}{||u(x, 0.5, 0.5) - u_{2^{k+2},2^{k+2},2^{k+2}}(x, 0.5, 0.5)||_\infty}.$$

5.4.1 Example [7]

Consider the following non-homogeneous semi-linear two-dimensional fractional reaction-diffusion model as

$$\frac{\partial u(x,y,t)}{\partial t} = D(\frac{\partial^{2\alpha} u(x,y,t)}{\partial |x|^{2\alpha}} + \frac{\partial^{2\alpha} u(x,y,t)}{\partial |y|^{2\alpha}}) - F(u) + f(x,y,t),\ 0 < \alpha \leq 1, \quad (5.17)$$

where $F(u) = u^2$ and $\Omega = [0,1] \times [0,1]$, with initial and boundary conditions as

$$u(x,y,0) = x^2(1-x)^2y^2(1-y)^2,\ (x,y) \in \Omega, \quad (5.18)$$

$$u(x,y,t) = 0,\ (x,y) \in \partial\Omega,\ 0 < t \leq 1, \quad (5.19)$$

and

$$\begin{aligned} f(x,y,t) = {} & -e^{-t}x^2(1-x)^2y^2(1-y)^2 + e^{-2t}x^4(1-x)^4y^4(1-y)^4 \\ & + \frac{0.5D}{cos(\alpha\pi)}e^{-t}y^2(1-y)^2(\frac{24(x^{4-2\alpha}+(1-x)^{4-2\alpha})}{\Gamma(5-2\alpha)} - \frac{12(x^{3-2\alpha}+(1-x)^{3-2\alpha})}{\Gamma(4-2\alpha)} \\ & + \frac{2(x^{2-2\alpha}+(1-x)^{2-2\alpha})}{\Gamma(3-2\alpha)}) + \frac{0.5D}{cos(\alpha\pi)}e^{-t}x^2(1-x)^2(\frac{24(y^{4-2\alpha}+(1-y)^{4-2\alpha})}{\Gamma(5-2\alpha)} \\ & - \frac{12(y^{3-2\alpha}+(1-y)^{3-2\alpha})}{\Gamma(4-2\alpha)} + \frac{2(y^{2-2\alpha}+(1-y)^{2-2\alpha})}{\Gamma(3-2\alpha)}). \end{aligned} \quad (5.20)$$

The analytic solution of equation (5.17) under the prescribed initial and boundary conditions is given as $u(x,t) = e^{-t}x^2(1-x)^2y^2(1-y)^2$.

A comparison of the analytical solution given in [163] and fast compact implicit integration factor (FcIIF) for $D = 0.5, \alpha = 0.8$ and for a fixed $y = 0.5$ at $t = 0.125$ is shown in Figure 5.1, which clearly exhibits that the analytic solution and the solution obtained by the proposed numerical scheme are in great agreement. The non-uniform meshes of time are taken as $t_n = (n/4)^s$ with $s = 3$.

Variations of solute concentration *vs.* x for $\alpha = 0.6, 0.7, 0.8$ for $D = 0.5$ and fixed value of $y = 0.5$ at $t_1 = (1/4)^3$, $t_2 = (2/4)^3$, $t_3 = (3/4)^3$ are shown through Figure 5.2. It is seen that the overshoots of the solute concentration decreases as the time taken for non-uniform meshes increases and also as the values of fractional derivative increases. The figure also depicts that the numerical solutions obtained by the proposed numerical scheme are in complete agreement with the results obtained from the analytical solutions.

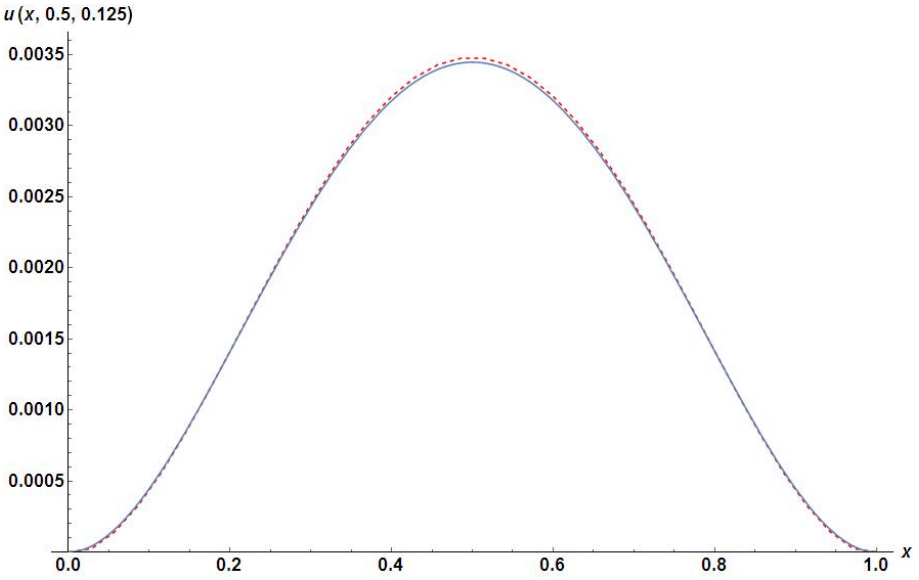

Figure 5.1: Comparison of analytical solution and numerical results obtained by using FcIIF for Example 5.4.1 for $D = 0.5, \alpha = 0.8$ and $y = 0.5$ at $t = 0.125$.

N	$\alpha = 0.6$	$\alpha = 0.7$	$\alpha = 0.9$
2^3	5.9328×10^{-4}	2.11131×10^{-5}	7.78134×10^{-6}
2^4	3.8241×10^{-5}	1.82825×10^{-5}	1.83512×10^{-7}
2^5	9.9428×10^{-6}	5.3588×10^{-6}	2.06951×10^{-8}

Table 5.1 L^∞-error non-uniform mesh ($s = 3$) for the SFRDE in Example 5.4.1 for different values of N and α.

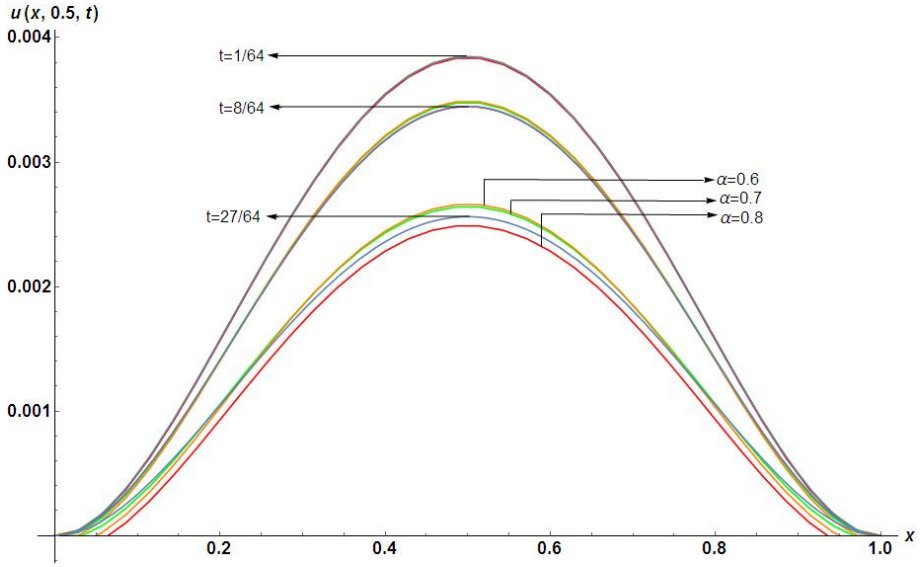

Figure 5.2: Comparison of the analytical solutions and results obtained by FcIIF for $\alpha = 0.6, 0.7, 0.8$ and $D = 0.5$, $y = 0.5$ at $t_1 = (1/4)^3, t_2 = (2/4)^3, t_3 = (3/4)^3$.

Table 5.1 shows how well the proposed FcIIF method work for Example 5.4.1. On non-uniform meshes, the numerical findings also shows that the FcIIF method is more accurate. It is found from the Table 5.1 that the L^∞-error of the concerned mathematical model (5.17) for different values of N clearly depicts that the proposed method FcIIF is stable for solving FPDEs. The accuracy can be increased as the values of N increase. The three dimensional plot of the solution profile *vs.* x and $y \in [0, 1]$, for $\alpha = 0.8$ at $t = 0.125$ is shown through Figure 5.3. For the rate of convergence, let us define $\mu_1 = \dfrac{||u(x, 0.5, 0.5) - u_{16,16,16}(x, 0.5, 0.5)||_\infty}{||u(x, 0.5, 0.5) - u_{8,8,8}(x, 0.5, 0.5)||_\infty} = 0.865931$ and $\mu_2 = \dfrac{||u(x, 0.5, 0.5) - u_{32,32,32}(x, 0.5, 0.5)||_\infty}{||u(x, 0.5, 0.5) - u_{16,16,16}(x, 0.5, 0.5)||_\infty} = 0.2931108$, here it is noticed that both μ_1 and μ_2 lies inside (0,1) interval, and since $\mu_1 > \mu_2$, it may be concluded that as k increases, μ_k decreases and $\mu_k \to 0$ as $k \to \infty$. This property indicates that the convergences of the considered model is superlinear and this can also be seen from Figure 5.4.

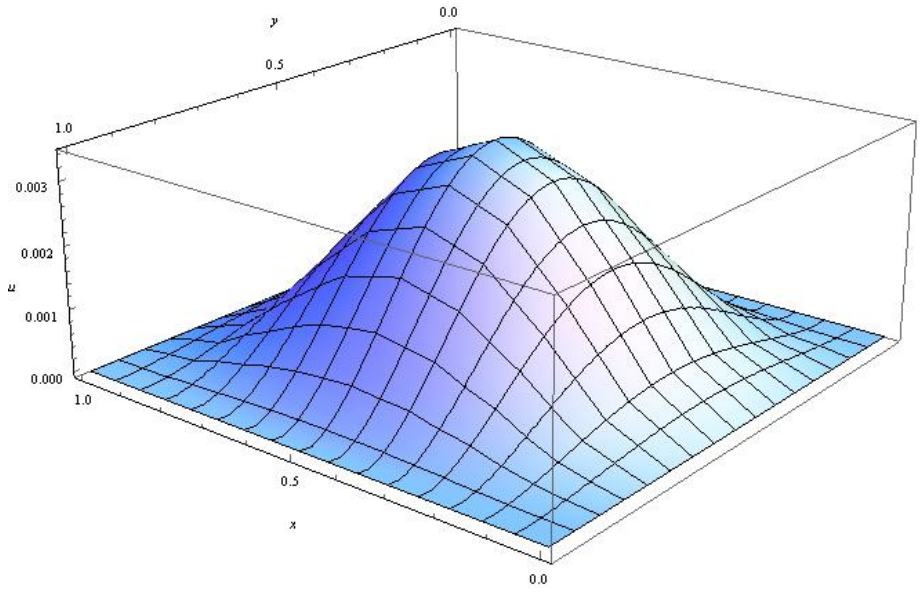

Figure 5.3: Variation of $u(x, y, t)$ *vs.* x and y for $\alpha = 0.8$ at $t = 0.125$.

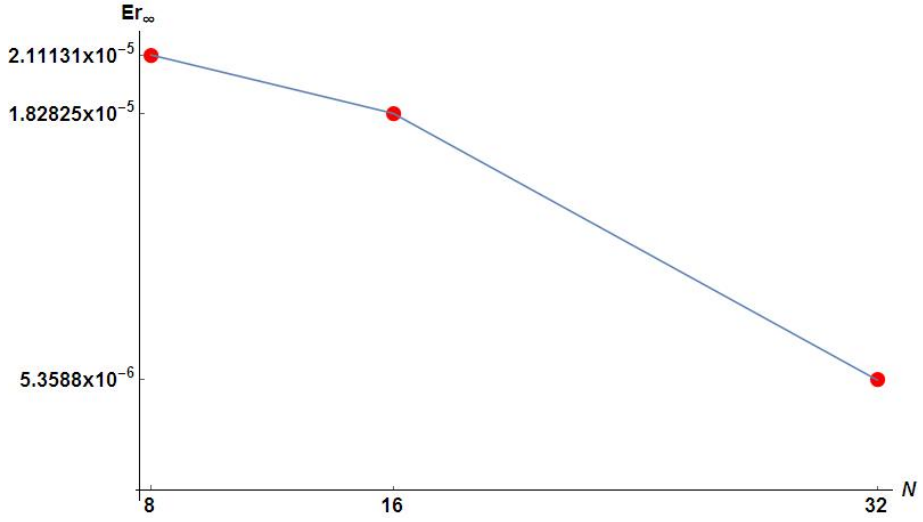

Figure 5.4: Log plot of L^{∞}-error on [0,1] with $\alpha = 0.7$ for Example 5.4.1 with y = 0.5, t = 0.5 Vs. N.

5.4.2 Example [8]

Consider the Fisher's type equation as

$$\frac{\partial u(x,y,t)}{\partial t} = 0.5\frac{\partial^{2\alpha} u(x,y,t)}{\partial |x|^{2\alpha}} + 0.75\frac{\partial^{2\alpha} u(x,y,t)}{\partial |y|^{2\alpha}} + f(u) + g(x,y,t), \tag{5.21}$$

where $f(u) = 0.1u(1-u)$, $0 < \alpha \leq 1$ and $\Omega = (0,1) \times (0,1)$, and

$$g(x,y,t) = -110e^{-t}x^2(1-x)^2y^2(1-y)^2 + 10^3e^{-2t}x^4(1-x)^4y^4(1-y)^4 + \frac{0.5y^2(1-y)^2}{cos(\alpha\pi)}(P(x,\alpha)+Q(x,\alpha)) + \frac{0.75x^2(1-x)^2}{cos(\alpha\pi)}(P(y,\alpha)+Q(y,\alpha)), \quad (5.22)$$

with

$$P(s,z) = 100\frac{e^{-t}s^{2-2z}}{\Gamma(3-2z)}(1 - \frac{6s}{3-2z} + \frac{12s^2}{(3-2z)(4-2z)}), \quad (5.23)$$

$$Q(s,z) = 100\frac{e^{-t}(1-s)^{2-2z}}{\Gamma(3-2z)}(1 - \frac{6(1-s)}{3-2z} + \frac{12(1-s)^2}{(3-2z)(4-2z)}). \quad (5.24)$$

The analytic solution of the equation (5.21) with the prescribed initial and boundary conditions as

$$u(x,y,0) = 100x^2(1-x)^2y^2(1-y)^2, \ (x,y) \in \Omega, \quad (5.25)$$

$$u(x,y,t) = 0, \ (x,y) \in \partial\Omega, \ 0 < t \leq 1, \quad (5.26)$$

is $u(x,t) = 100e^{-t}x^2(1-x)^2y^2(1-y)^2$ as given in [8]. Let us repeat the entire procedure as applied in Example 5.4.1. Figure 5.4 depicts a comparison between the analytical solution [163] and the proposed numerical scheme FcIIF for $\alpha = 0.8$ and for a fixed $y = 0.5$ at $t = 0.125$. It is observed from the figure that the results are quite similar as in Example 5.4.1, where the non-uniform meshes of time are taken as $t_n = (n/4)^s$ with $s = 3$.

The variation of solute concentration *vs.* x is shown through Figure 5.5, for fixed $y = 0.5$ at $t_1 = (1/4)^3$, $t_2 = (2/4)^3$, $t_3 = (3/4)^3$ for $\alpha = 0.6, 0.7, 0.8$ and 0.9, and for fixed $y = 0.5$ and $D = 0.5$. The nature of concentration is similar to Example 5.4.1

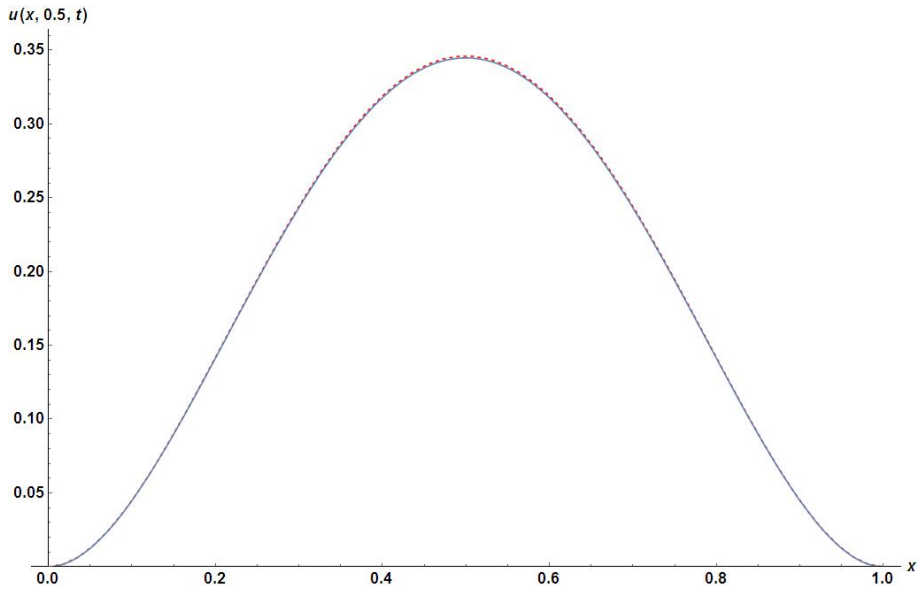

Figure 5.5: Comparison of analytical solution and numerical solution using FcIIF for Example 5.4.2 at $\alpha = 0.8$ and $y = 0.5$ for $t = 0.125$.

with a difference that here the concentration is higher as compared to the previous example.

N	$\alpha = 0.6$	$\alpha = 0.7$	$\alpha = 0.9$
2^3	3.82981×10^{-3}	3.41542×10^{-3}	2.94219×10^{-4}
2^4	2.91548×10^{-3}	2.4219×10^{-3}	5.2487×10^{-4}
2^5	7.91452×10^{-4}	7.84592×10^{-4}	3.911102×10^{-5}

Table 5.2 L^∞-error non-uniform mesh ($s = 3$) for the SFRDE in Example 2 for different values of N and α.

Table 5.2 shows the effectiveness of the proposed FcIIF method for Example 5.4.2. The numerical findings in Table 5.2 also suggest that the FcIIF method is more accurate on non-uniform models. The L^∞-error for $\alpha = 0.6, 0.7, 0.9$, $N = 2^3, 2^4, 2^5$, $y = 0.5$ at $t = 0.5$ given in Table 5.2 clearly exhibits the accuracy of our proposed numerical scheme with the analytic solution of the mathematical model (5.21).

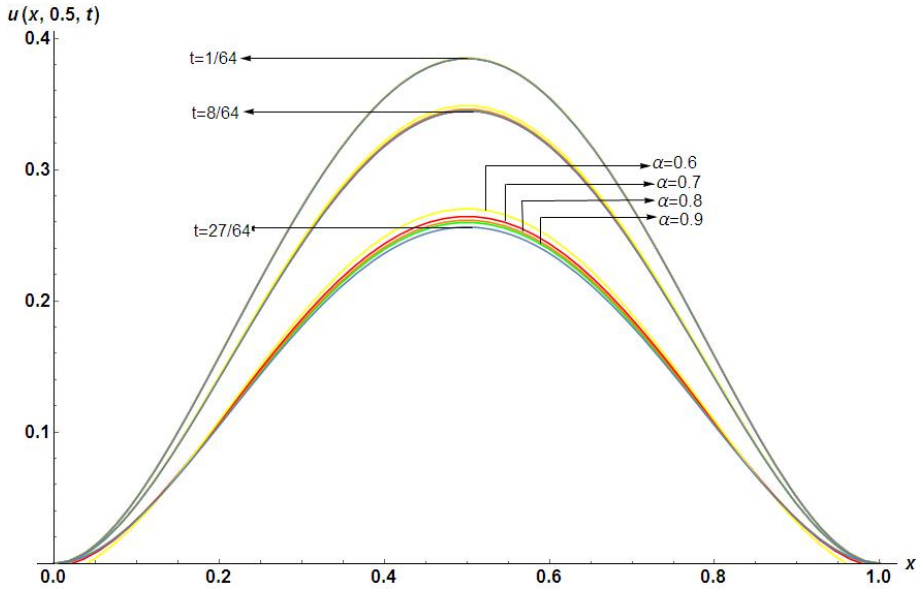

Figure 5.6: Comparison of the analytical solution and numerical solution using FcIIF for $\alpha = 0.6, 0.7, 0.8, 0.9$ for a fixed $y = 0.5$ at $t_1 = (1/4)^3$, $t_2 = (2/4)^3$, $t_3 = (3/4)^3$.

The accuracy can be increased with the increase in N. The numerical values of the solute concentration obtained by the analytical result and the proposed method FcIIF against α for different time t are shown through Figure 5.6. The Figure 5.7 depicts the three dimensional plot of $u(x, y, 0.125)$ $vs.$ x, $y \in$[0,1] for $\alpha = 0.8$.

As in Example 5.4.1, it is seen the similar behavior in this example, that is, $\mu_1 = 0.7091075$ and $\mu_2 = 0.324505$, here we notice both μ_1 and μ_2 lies inside (0,1) interval, and since $\mu_1 > \mu_2$, it may be concluded that as k increases, μ_k decreases and $\mu_k \to 0$ as $k \to \infty$. This property indicates that the convergences of the considered model is superlinear and this can also be seen from Figure 5.9.

5.5 Results and discussion

In this section, a drive has been made to use the proposed validated numerical scheme to solve the concerned two-dimensional non-linear fractional order partial

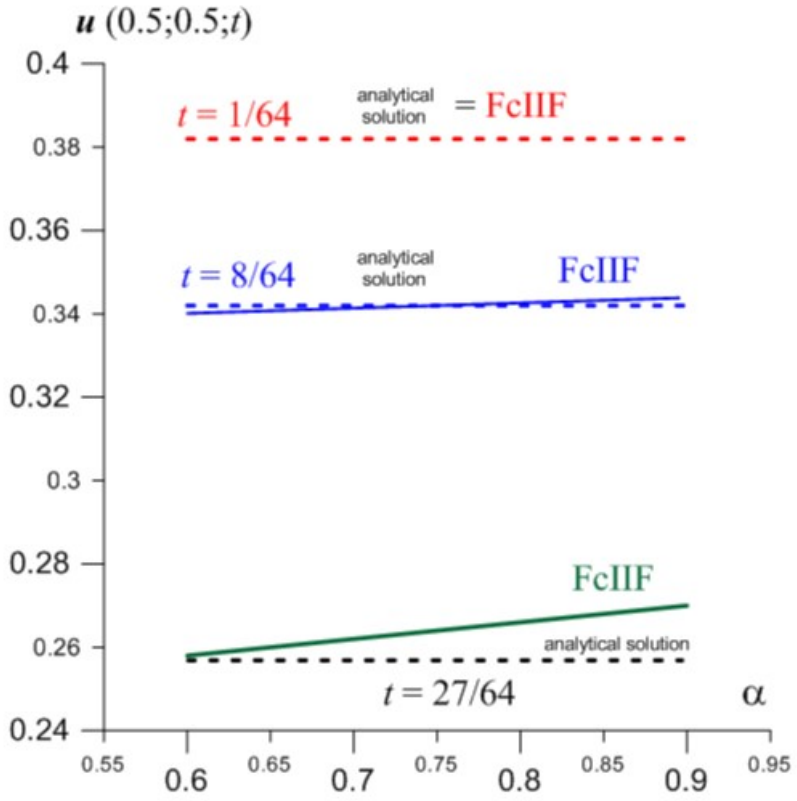

Figure 5.7: Variations of the solute concentration $u(0.5, 0.5, t)$ *vs.* α obtained for the analytical solution (continuous line) and FcIIF (broken line) for different values of α.

differential equation with Riesz space fractional derivative (RSFDE) as

$$\frac{\partial u(x,y,t)}{\partial t} = D(\frac{\partial^{\beta+1}u(x,y,t)}{\partial|x|^{\beta+1}} + \frac{\partial^{\beta+1}u(x,y,t)}{\partial|y|^{\beta+1}}) - V_x\frac{\partial^{\beta}u(x,y,t)}{\partial|x|^{\beta}} - V_y\frac{\partial^{\beta}u(x,y,t)}{\partial|y|^{\beta}} - u(1-u),\ 0<\beta<1, \tag{5.27}$$

under the prescribed initial condition and boundary conditions given by

$$u(x,y,0) = 1;\ (x,y)\in\Omega,\ u(x,y,t) = 0;\ (x,y)\in\partial\Omega,\ 0<t\leq 1. \tag{5.28}$$

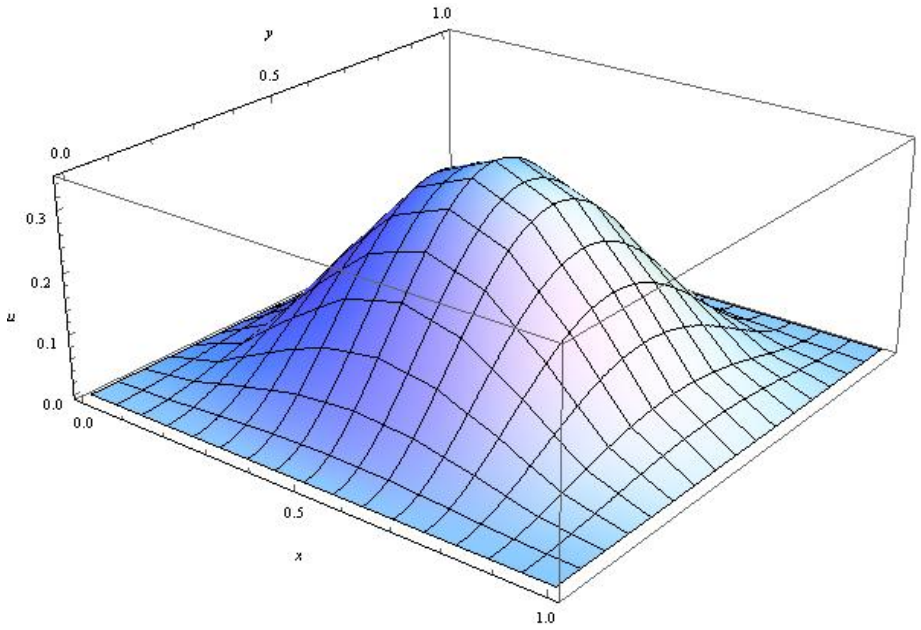

Figure 5.8: Variation of $u(x, y, t)$ *vs.* x and y, for $\alpha = 0.8$ at $t = 0.125$.

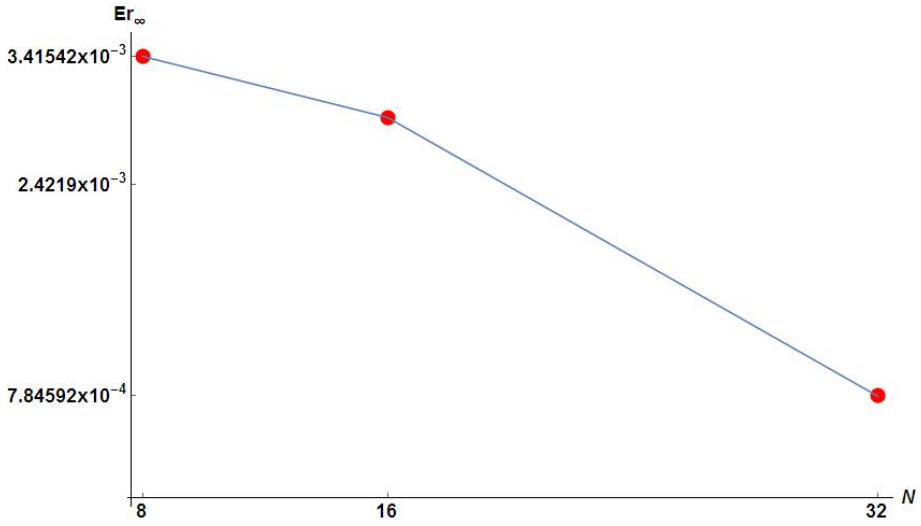

Figure 5.9: Log plot of L^{∞}- error on [0,1] with $\alpha = 0.7$ for Example 5.4.2 with y = 0.5, t = 0.5 Vs. N

If $V_x = V_y \neq 0$, the equation (5.27) is known as SFRADE, while for $V_x = V_y = 0$, the equation (5.27) is called as SFRDE. The aim is to find the solution of the problem using the proposed numerical scheme for both the cases and to show the effect of damping due to the presence of reaction term for different values of Riesz fractional

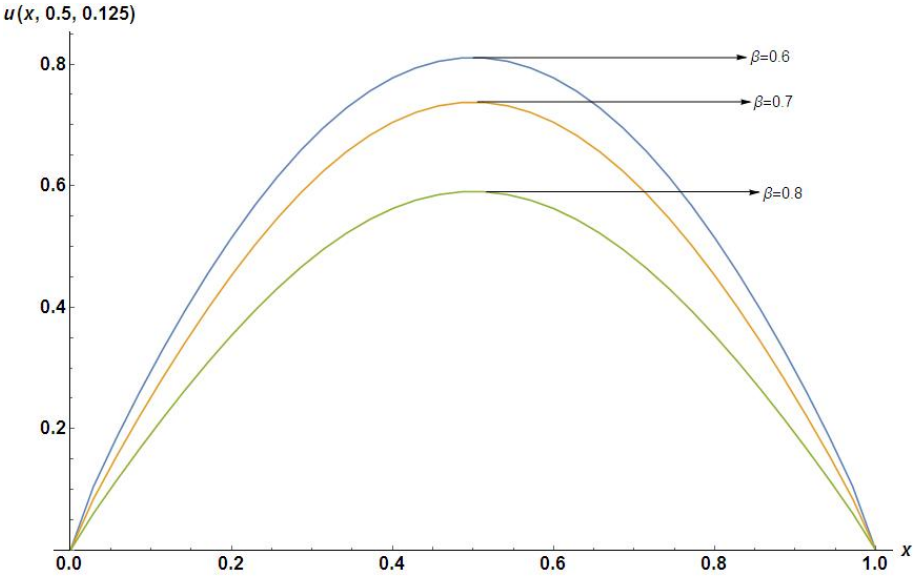

Figure 5.10: Plots of solutions of the SFRDE given in equation (5.27) for different values of β for $V_x = V_y = 0.6$, $y = 0.5$ at $t = 0.125$.

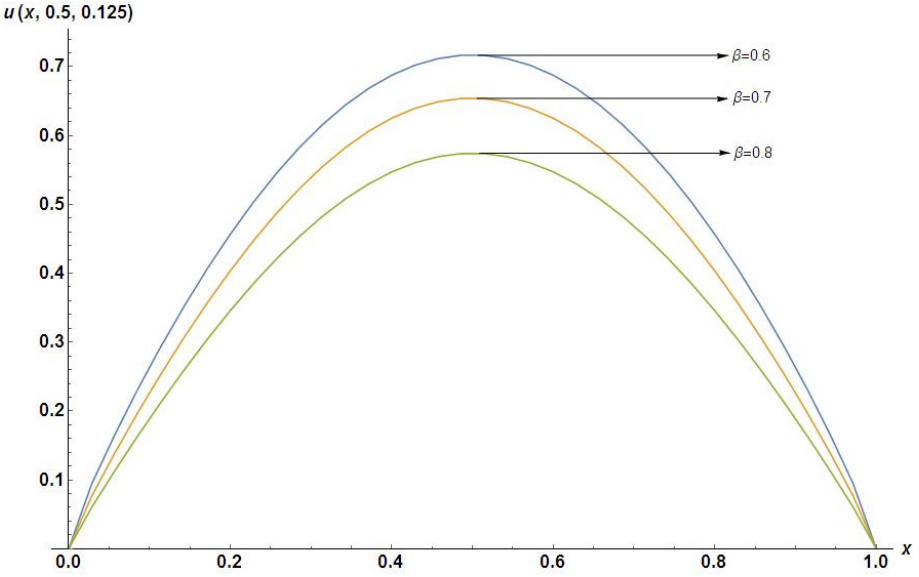

Figure 5.11: Plots of solutions of the SFRDE given in equation (5.27) for different values of β for $V_x = V_y = 0.3$, $y = 0.5$ at $t = 0.125$.

order derivative taking the diffusivity constant as $D = 1$.

Figures 5.10-5.12 are drawn to show the variations of solution profile $u(x, y, t)$ *vs.* x for $y = 0.5$, $t = 0.125$ for different values of Riesz derivative β. It is seen from

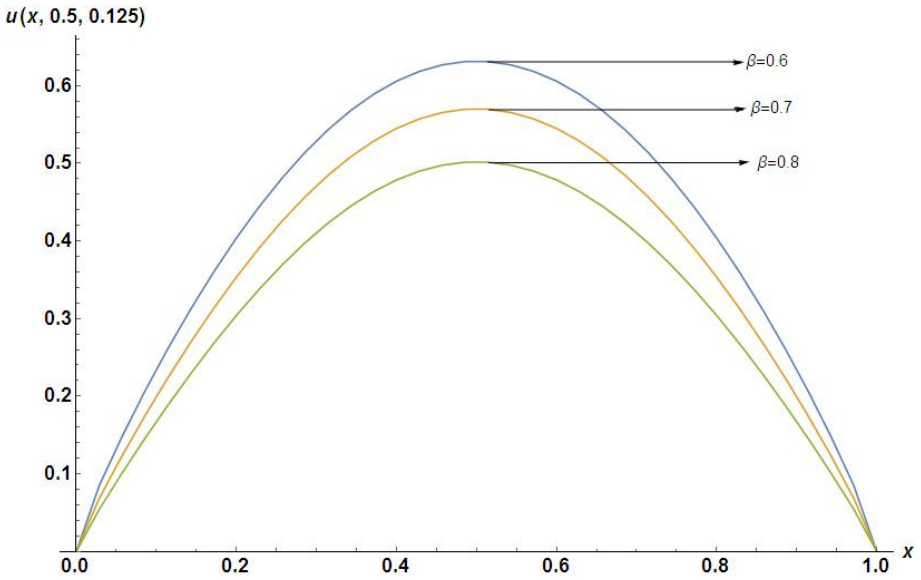

Figure 5.12: Plots of solutions of the SFRDE given in equation (5.27) for different values of α for $V_x = V_y = 0$, $y = 0.5$ at $t = 0.125$.

Figures 5.10-5.12 that the nature of the graphs is similar. In all the cases, sub-diffusions are clearly found with the overshoots close to $x = 0.5$. Figure 5.10 and Figure 5.11 are showing the damping of the solution profiles for $V_x = V_y = 0.6$ and $V_x = V_y = 0.3$, respectively. It is clearly seen from the figures that in both the occasions, the damping is less as compared to SFRADE i.e., when $V_x = V_y = 0$, which are shown through Figure 5.12. The damping nature of solute concentration *vs.* $\alpha = \beta + 1$ for the concerned model (5.27) for different values of the advection coefficients is shown through Figure 5.13, which clearly predicts that the concentration increases with the increase in values of the advection coefficients.

5.6 Conclusion

The numerical method named as fast compact implicit integration factor (FcIIF) method with non-uniform time meshes, is used to solve the two-dimensional nonlinear Riesz space-fractional reaction-diffusion equation. It is found that this method

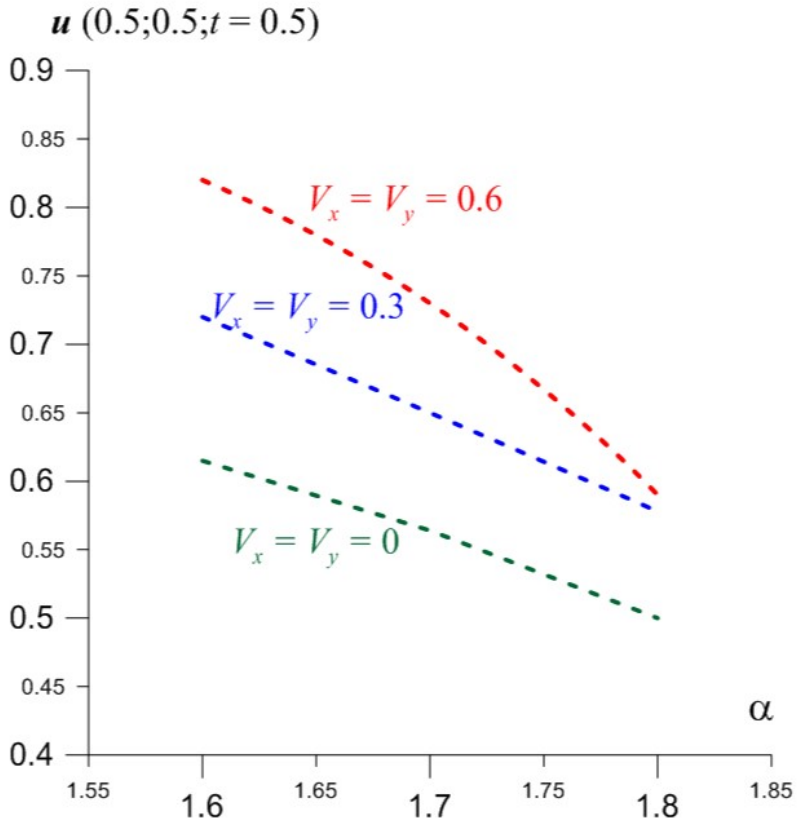

Figure 5.13: Damping effect of solute concentration $u(0.5, 0.5, t = 0.5)$ *vs.* $\alpha = \beta + 1$ for the SFRDE, given in (5.27) for various values of advection coefficients V_x, V_y.

has great accuracy and stability for second order scheme. Validation of the effectiveness of the proposed method is shown through graphs and tables while applying it in the existing problems having analytic solutions. Since the numerical scheme deals with diagonal matrices that reduces the computational cost as well as the computational time and also since time meshes are non-uniform, the accuracy of the solution is more as compared to the method of uniform meshes. The method and techniques discussed in this chapter can also be applied to solve other kinds of fractional order partial differential equations which have importances in the real physical world.

****